Journal of Alloys and Compounds 517 (2012) 127–131

Contents lists available at SciVerse ScienceDirect

Journal of Alloys and Compounds

journal homepage: www.elsevier.com/locate/jallcom

Hydrogen storage properties of $LiBH_4$–Li_3AlH_6 composites

Xiaocheng Wu[a], Xinhua Wang[a,*], Guozhou Cao[c], Shouquan Li[a], Hongwei Ge[a], Lixin Chen[a], Mi Yan[b,*]

[a] Department of Materials Science and Engineering, Zhejiang University, Hangzhou 310027, China
[b] State Key laboratory of Silicon Materials, Zhejiang University, Hangzhou 310027, China
[c] Ningbo Entry-Exit Inspection and Quarantine Bureau Technical Center, Ningbo 315000, China

ARTICLE INFO

Article history:
Received 5 September 2011
Received in revised form
12 December 2011
Accepted 13 December 2011
Available online 22 December 2011

Keywords:
Hydrogen storage materials
Complex hydrides
Hydrogen storage properties
Hydrogen

ABSTRACT

To improve the dehydrogenation properties of $LiBH_4$, a novel hydrogen storage system, $LiBH_4$–Li_3AlH_6, was synthesized by mechanical ball milling. The dehydrogenation/rehydrogenation properties of $LiBH_4$–Li_3AlH_6 (molar rato: 1:1) composites were studied via thermogravimetry (TG), differential scanning calorimetry (DSC), mass spectral analysis (MS), powder X-ray diffraction (XRD), and Fourier transform infrared spectroscopy (FTIR). The experimental results show that the hydrogen desorption capacity reaches 8.5 wt% and that the whole dehydrogenation is a three-step process: (1) a decomposition reaction $Li_3AlH_6 \rightarrow 3LiH + Al + 3/2H_2$, occurring at 160 °C; (2) formation of an intermediate product from 300 °C to 350 °C, and then subsequent transformation into Al, AlB_2, and H_2. ($2LiBH_4 + Al \rightarrow [Li_2B_2AlH_4] \rightarrow x(AlB_2 + 2LiH + 3H_2) + (1-x)$ $[Li_2B_2AlH_4]$, $(0<x<1)$); and (3) final dehydrogenation of $LiH + Al \rightarrow LiAl + 1/2H_2$, occurring at 415 °C, with sequential decomposition of the remaining intermediate ($(1-x)[Li_2B_2AlH_4] \rightarrow (1-x)(AlB_2 + 2LiH + 3H_2)$, $(0<x<1)$). Furthermore, the dehydrogenated products can be rehydrogenated to LiBH4 at 8 MPa H_2 and 400 °C.

1. Introduction

Hydrogen as an energy vector is taking more and more important action in the world energy systems because of its non-polluting characteristics. One of the key steps for the application of hydrogen energy is the development of appropriate hydrogen storage materials that have extremely high gravimetric and volumetric hydrogen storage densities, and perfect reversibility. In 2009, the U.S. Department of Energy (DOE) set final targets of 7.5 wt% (gravimetric hydrogen density) and 70 g H_2 L^{-1} (volumetric hydrogen density) for the vehicular application of hydrogen storage materials [1]. Traditional metal hydrides (e.g., $LaNi_5$, TiFe, $TiMn_2$) have relatively low hydrogen storage capacity, thus cannot meet the requirements of vehicular application of hydrogen storage systems. The research and development of new hydrogen storage materials with high hydrogen storage capacity and good reversibility is of great importance for the improvement of vehicular hydrogen storage systems.

Over the past few years, many studies have been focused on solid-state hydrogen storage materials using complex hydrides, including alanates, borohydrides, amide hydrides, and combinations thereof [2–21]. Among these hydrides, lithium borohydride ($LiBH_4$) is a potential hydrogen storage material due to its large theoretical hydrogen capacity (18.5 wt%). Unfortunately, $LiBH_4$ is thermodynamically stable, the main evolution of hydrogen starts above 380 °C, and only half of the hydrogen can be released below 600 °C [18–20]. Furthermore, the conditions for forming $LiBH_4$ from its dehydrogenated products are rigorous (15.5 MPa H_2, 600 °C) [22]. Therefore, novel strategies and methods must be found to improve the hydrogen storage properties of $LiBH_4$. Some groups [23–25] proposed the destabilization of $LiBH_4$ by Al, and the results indicate that the decomposition of $LiBH_4$ starts at a lower temperature (320 °C) than pure $LiBH_4$ and that rehydrogenation can be achieved under conditions of 15 MPa H_2 and 350 °C (reaction (1)).

$$2LiBH_4 + Al \leftrightarrow AlB_2 + 2LiH + 3H_2 \quad (1)$$

However, Al powders in the reaction easily form oxide layers which prevent Al from reacting with $LiBH_4$. For this reason, a $LiBH_4$–$LiAlH_4$ system was reported [26,27]. Furthermore, Li_3AlH_6 is a good candidate hydrogen storage material [28–30]. Unfortunately, to the best of our knowledge, few papers related to $LiBH_4$–Li_3AlH_6 system have been reported.

In the present work, the hydrogen storage performance of the $LiBH_4$–Li_3AlH_6 composite (molar ratio: 1:1) without any additives is investigated. The pathways of dehydrogenation/rehydrogenation and reversibility of $LiBH_4$–Li_3AlH_6 composite are discussed. The above studies would be helpful in improving the properties of Li–Al–B–H systems.

* Corresponding authors. Tel.: +86 571 87952716; fax: +86 571 87952716.
E-mail addresses: xinhwang@zju.edu.cn (X. Wang), mse_yanmi@zju.edu.cn (M. Yan).

0925-8388/$ – see front matter © 2011 Elsevier B.V. All rights reserved.
doi:10.1016/j.jallcom.2011.12.054

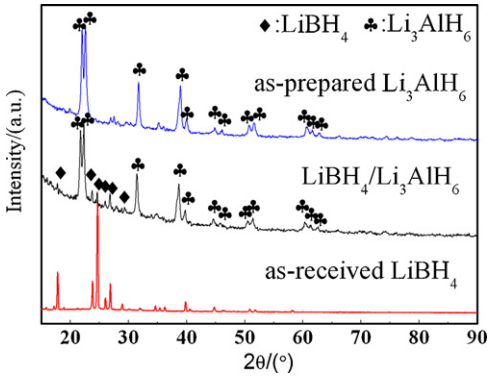

Fig. 1. XRD patterns of as-prepared Li_3AlH_6, as-received $LiBH_4$ and $LiBH_4/Li_3AlH_6$.

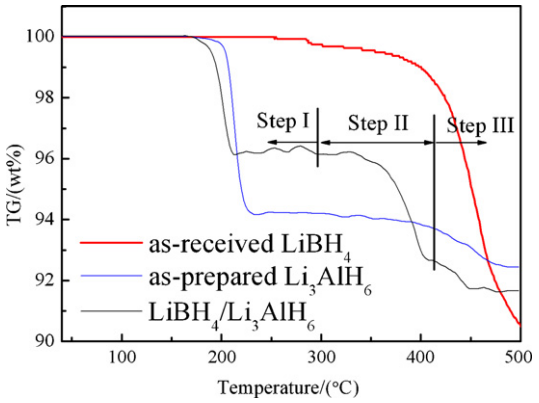

Fig. 2. The comparison of TG curves for as-received $LiBH_4$, as-prepared Li_3AlH_6 and $LiBH_4/Li_3AlH_6$ composite at a heating rate of 5 °C min^{-1}.

2. Experimental

2.1. Sample preparation

Lithium borohydride ($LiBH_4$, 95%, powder, Acros Organics), lithium alanate ($LiAlH_4$, 97%, powder, Alfa Aesar), and lithium hydride (LiH, 98%, powder, Alfa Aesar) were used as received without further purification. All sample storage and handling were performed in a Mikrouna glove box filled with high-purity argon (Ar, 99.999%) and controlled H_2O (<0.5 ppm) and O_2 (<0.1 ppm) concentrations. QM-3SP4 planetary ball mill is used to prepare Li_3AlH_6 and $LiBH_4/Li_3AlH_6$ composites.

Li_3AlH_6 was synthesized through the mechanochemical reaction between LiH and $LiAlH_4$. LiH and $LiAlH_4$, with a molar ratio of 2:1, were loaded into a 100-ml stainless milling pot (1Cr18Ni9Ti) with 25 steel balls (10 mm in diameter); the ball-to-powder weight ratio is about 45:1. Ball milling was performed for 6 h under a 0.1 MPa argon atmosphere, and the rotation speed is 500 rpm. $LiBH_4/Li_3AlH_6$ composites without any additives were prepared by ball milling a mixture of $LiBH_4$ and Li_3AlH_6 (molar ratio: 1:1) for 0.5 h under a 0.1 MPa argon atmosphere.

2.2. Sample characterization

Non-isothermal dehydrogenation was investigated using a Netzsch STA449F3 synchronous thermal analysis (thermogravimetry/differential scanning calorimetry (TG/DSC)) system equipped with a Netzsch QMS403C mass spectrometer (MS) at a heating rate of 5 °C min^{-1} in a flow of high purity Ar (50 ml min^{-1}).

Investigations of dehydriding/hydriding reversibility were carried out on a Sieverts-type apparatus [31–33]. About 0.2 g of the sample was loaded into a stainless holder connected to a thermocouple to control the sample temperature. Hydrogenation measurements were performed under 8 MPa H_2 by heating from room temperature to 400 °C at a rate of 5 °C min^{-1}, and then holding at 400 °C for 300 min.

Powder X-ray diffraction (XRD) analysis was carried out using a PANalytical X-ray diffractometer (X'Pert PRO, Cu-Kα, 3 kW). Samples were mounted onto a 1-mm-deep glass board in an Ar-filled glove box and sealed with an amorphous membrane to avoid oxidation during the XRD measurements.

Infrared measurements were performed on a Beuker-Vector22 Fourier transform infrared spectroscope (FTIR) in transmission mode. The samples were pressed with potassium bromide (KBr) powder at a weight ratio of 1:99 to form a pellet. To avoid oxidation, a specially designed sample holder, which could fill with Ar, was used for FTIR measurements. The sample preparation and transformation are carried out in an Ar-filled glove box.

All the samples for XRD and FTIR measurements were cooled to room temperature after isothermal dehydrogenation under 0.01 MPa hydrogen at different temperatures (T = 160, 220, 250, 300, 350, 415, 450, and 500 °C)

3. Results and discussion

3.1. Dehydrogenation performance

The XRD patterns of as-prepared Li_3AlH_6, as-received $LiBH_4$, and as-milled $LiBH_4/Li_3AlH_6$ are shown in Fig. 1, from which it can be seen that after $LiBH_4$ and Li_3AlH_6 (molar ratio: 1:1) are mixed and ball milled for 0.5 h, the characteristic diffraction peaks of $LiBH_4$ and Li_3AlH_6 remain, and no other diffraction peaks are detected. However, the intensity of the peaks of both $LiBH_4$ and Li_3AlH_6 decrease. This suggests that $LiBH_4$ and Li_3AlH_6 do not interact with each other during ball milling.

Fig. 2 shows the non-isothermal dehydrogenation performances of as-received $LiBH_4$, as-prepared Li_3AlH_6, and as-milled $LiBH_4/Li_3AlH_6$ heated from room temperature to 500 °C at a heating rate of 5 °C min^{-1}. The as-milled $LiBH_4/Li_3AlH_6$ clearly shows three-step hydrogen release. The first step begins at 160 °C, which is 20 °C lower than the initial decomposition temperature of Li_3AlH_6. The particle size reduction may be one of the main reasons for the decrease. Approximately 3.9 wt% (Fig. 3) of hydrogen could be released before 215 °C. In the second step, hydrogen is released over a larger temperature range from 300 to 420 °C, and the hydrogen desorption capacity reaches 3.7 wt% (Fig. 3). A fluctuation is observed in the TG curve of $LiBH_4/Li_3AlH_6$ in the temperature range of 215–300 °C, which is caused by the fusion of $LiBH_4$. After this fluctuation, the TG curve of the $LiBH_4/Li_3AlH_6$ composite dipped, corresponding to the weight loss of the composite. This indicates that the second hydrogen-release step begin after the fluctuation at 300 °C. After heating to 415 °C, the third step of dehydrogenation occurs with 0.8 wt% hydrogen released.

Fig. 3 presents the TG/DSC/MS curves of the $LiBH_4/Li_3AlH_6$ composite at a heating rate of 5 °C min^{-1}. In the DSC curve, five endothermic peaks during the dehydrogenation of the $LiBH_4/Li_3AlH_6$ composite are observed. The peak maxima are at 112, 205, 272, 395, and 445 °C. Among them, peaks at 112 and 272 °C correspond to the structural transition and melting reaction

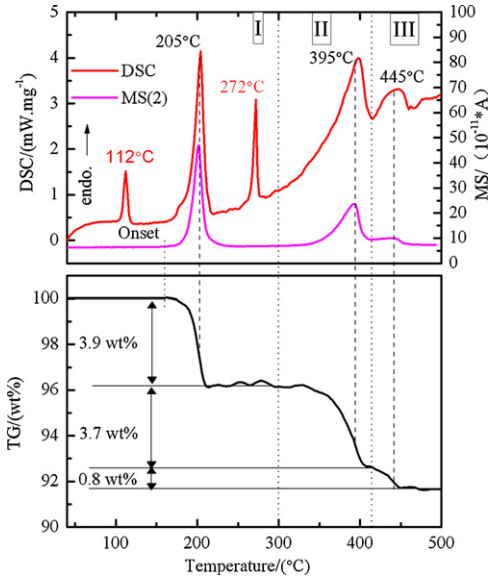

Fig. 3. TG/DSC/MS curves of $LiBH_4/Li_3AlH_6$ composite at a heating rate of 5 °C min^{-1}.

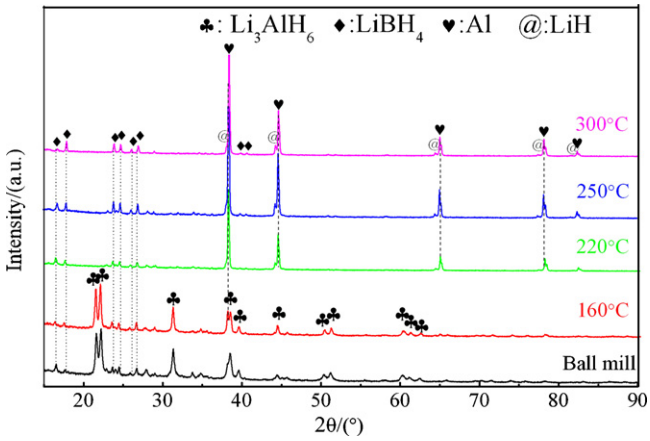

Fig. 4. XRD patterns for the $LiBH_4/Li_3AlH_6$ composite obtained at different temperatures (160, 220, 250, and 300 °C) and ball milled sample.

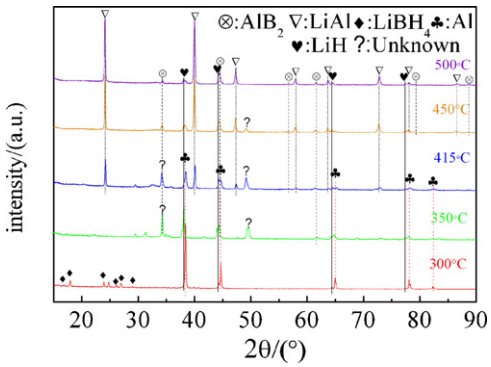

Fig. 5. XRD patterns for the $LiBH_4/Li_3AlH_6$ composite obtained at different temperatures (300, 350, 415, 450, and 500 °C).

temperatures of $LiBH_4$, respectively, which are in good agreement with the results reported in the literature [17,34]. In the MS curve, three peaks for hydrogen release are observed, corresponding to weight losses at 205, 395, and 445 °C in the TG curve. This suggests that three reactions occurred at 205, 395, and 445 °C lead to hydrogen release in the three-step dehydrogenation of the $LiBH_4/Li_3AlH_6$ composite.

3.2. Dehydrogenation mechanism

From Fig. 2 it seems that the first step dehydrogenation curve of $LiBH_4/Li_3AlH_6$ composite is similar to the decomposition curve of Li_3AlH_6. This leads us to suppose that the first dehydrogenation step of $LiBH_4/Li_3AlH_6$ composite is mainly caused by the decomposition of Li_3AlH_6 (reaction (2)), and that $LiBH_4$ may not participate in the reaction at below 250 °C. Based on this supposition, the theoretical dehydrogenation capacity of $LiBH_4/Li_3AlH_6$ composite in the first dehydrogenation step is 4.0 wt%. The experimental hydrogen release capacity (3.9 wt%) in the first dehydrogenation stage of $LiBH_4/Li_3AlH_6$ composite agrees well with the above theoretical hydrogen capacity. In order to further confirm this mechanism, XRD analysis was carried out on the samples collected after isothermal dehydrogenation at various temperatures (160, 220, 250, and 300 °C), and the results are shown in Fig. 4. After the $LiBH_4/Li_3AlH_6$ composite was heated to 160 °C, no changes were observed for $LiBH_4$ and Li_3AlH_6, but the weak characteristic diffraction peaks of Al ($2\theta = 38.4°$) were detected. This suggests that Al begins to appear at the initial dehydrogenation temperature (160 °C). After heating to 220 °C more Al and LiH are formed, and the diffraction peaks of Li_3AlH_6 disappear. However, the diffraction peaks of $LiBH_4$ remain and no other boron (B)-related phases are observed at below 300 °C. These results indicate that Li_3AlH_6 is consumed by decomposition to Al and LiH according to reaction (2); $LiBH_4$ seems not participate in the reaction during the first dehydrogenation step. From Fig. 3 it can be seen that reaction (2) in the first dehydrogenation step of $LiBH_4/Li_3AlH_6$ composite is an endothermic reaction, which agrees with the results reported in the literature [29].

$$Li_3AlH_6 \rightarrow 3LiH + Al + 3/2H_2 \quad (2)$$

To understand the reaction pathways of the second and third dehydrogenation steps of the $LiBH_4/Li_3AlH_6$ composite, XRD analysis was carried out for the samples collected after heating to 300–500 °C. When the composite is heated to 350 °C, the diffraction peaks of $LiBH_4$ disappear, and the peaks of AlB_2 and an unknown phase (marked "?" in Fig. 5) are simultaneously detected. The results reveal that reaction (3) can continue and $LiBH_4$ can be turned into an intermediate product corresponding to the unknown phase. After the composite is heated to 415 °C, LiAl is gradually formed. The formation of LiAl is caused by reaction (4), which mainly leads to the third dehydrogenation step. The intensity of the Al diffraction peaks is obviously weakened and finally the peaks disappear at 500 °C, as shown in Fig. 5. This suggests that Al is gradually involved in the reaction with $LiBH_4$ and LiH during the second and third dehydrogenated steps. The diffraction peaks of LiH appear from 300 to 500 °C in Fig. 5. From Eqs. (2)–(4), it is easy to show that LiH, which is both a reactant and a product, is in excess during the dehydrogenation of the $LiBH_4/Li_3AlH_6$ composite. As shown in Fig. 3 a turn at around 415 °C in the TG curve is also observed, which is caused by reaction (4). The two endothermic peaks and two hydrogen release peaks at 395 and 445 °C in the DSC and MS curves of Fig. 3, correspond to reactions (3) and (4), respectively. The reaction temperature ranges of the two reactions in our work are consistent with those reported in the literature [23,35]. Based on reactions (3) and (4), the theoretical dehydrogenation capacities of the second and third dehydrogenation steps of the $LiBH_4/Li_3AlH_6$ composite were found to be 4.0 and 0.7 wt%, respectively. However, the experimental values for the second and third dehydrogenation steps yielded 3.7 and 0.8 wt%, respectively, as shown in Fig. 3. This suggested the decomposition of the intermediate product during the second and third dehydrogenation stages.

$$2LiBH_4 + Al \rightarrow AlB_2 + 2LiH + 3H_2 \quad (3)$$

$$LiH + Al \rightarrow LiAl + 1/2H_2 \quad (4)$$

The diffraction peaks of the unknown phase (marked as "?" in Fig. 5), which other researchers also found in their works [27,36], is found at 49.2° (2θ). As the temperature increases, the peak intensity first increases, gradually decreases from 415 to 450 °C, and then finally disappear at 500 °C. The strongest diffraction peaks of the AlB_2 phase theoretically occur at 44.4° (2θ), but the diffraction peaks detected at 34.1° (2θ), which also belong to AlB_2 phase, are stronger than the peaks at 44.4° (2θ) at 350 and 415 °C, as shown in Fig. 5. The intensity of the diffraction peaks at 34.1° (2θ) also gradually weakens, similar to the diffraction peaks at 49.2° (2θ). This result indicates that the diffraction peaks of the intermediate and AlB_2 overlapped at 34.1° (2θ). In addition, the diffraction peaks of $LiBH_4$ disappear and the diffraction peaks of Al weaken after heating to 350 °C. The unknown phase is likely to be the intermediate product, which is formed by $LiBH_4$ and Al from 300 to 350 °C and decomposed mostly into AlB_2, LiH, and H_2 in the second step (reaction (5)). The remaining intermediates decompose during the third dehydrogenation step (reaction (6)).

$$2LiBH_4 + Al \rightarrow [Li_2B_2AlH_4] \rightarrow x(AlB_2 + 2LiH + 3H_2) + (1-x)[Li_2B_2AlH_4],\ 0 < x < 1 \quad (5)$$

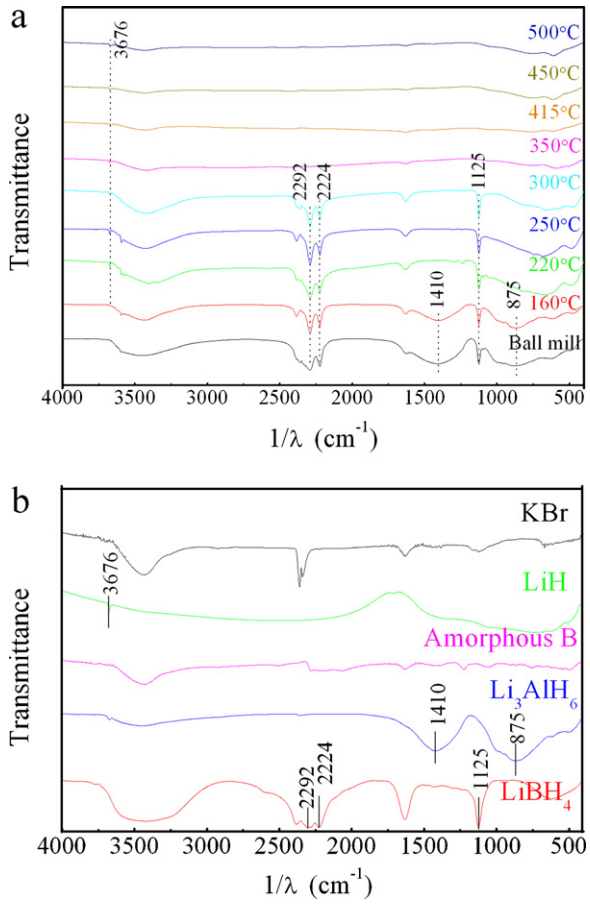

Fig. 6. FTIR spectra for (a) the $LiBH_4/Li_3AlH_6$ composite obtained at different temperatures (160, 220, 250, 300, 350, 415, 450, and 500 °C) and ball milled sample, and (b) related substances included KBr, LiH, amorphous B, Li_3AlH_6, and $LiBH_4$.

$$(1-x)[Li_2B_2AlH_4] \rightarrow (1-x)(AlB_2 + 2LiH + 3H_2),\ 0 < x < 1 \quad (6)$$

Fig. 6 shows the FTIR spectra of the $LiBH_4/Li_3AlH_6$ composite dehydrogenated at various temperatures. First, the vibrational peaks of Li_3AlH_6 (1410 and 875 cm^{-1}) disappear when the composite is heated to 220 °C. This means that Li_3AlH_6 decomposes according to reaction (2) before 220 °C, which is in good agreement with the XRD analysis (Fig. 3). Second, three characteristic vibrational peaks (2292, 2224, and 1125 cm^{-1}) of $LiBH_4$ are found below 300 °C, fading away when the temperature increased to 350 °C. This phenomenon indicates that $LiBH_4$ reacts with Al (reaction (5)) at the temperature range of 300–350 °C. Third, LiH, whose characteristic vibrational peak is at 3676 cm^{-1}, is found to exist in the temperature range of 160–500 °C, which is also in good agreement with the XRD analysis (Fig. 3). Fourth, as is known, the B phase of relevant dehydrogenated samples of $LiBH_4$ is usually amorphous [37]. No characteristic vibrational peaks corresponding to amorphous B are detected in the FTIR spectrum of the dehydrogenated samples. This means that the formation of amorphous B may be restrained by the formation of AlB_2.

In summary, the dehydrogenation of $LiBH_4/Li_3AlH_6$ composites below 500 °C is found to occur in three steps: (1) a decomposition reaction (reaction (2)), occurring at 160 °C; (2) formation of an intermediate product from 300 to 350 °C, and then subsequent transformation into Al, AlB_2, and H_2 (reaction (5)) during heating to 415 °C; and (3) final dehydrogenation (reaction (4)), occurring at 415 °C, with sequential decomposition of the remaining intermediate (reaction (6)).

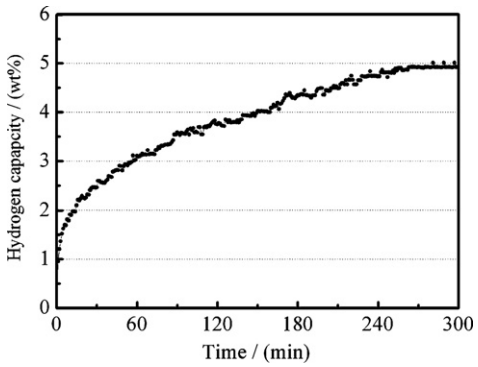

Fig. 7. The rehydrogenation curves of dehydrogenated $LiBH_4/Li_3AlH_6$ sample under 8 MPa H_2 at 400 °C.

3.3. Reversibility

The reversibility properties of the $LiBH_4/Li_3AlH_6$ composites were investigated. The rehydrogenation of the sample was conducted under 8 MPa H_2 at 400 °C after complete dehydrogenation. And the rehydrogenation kinetics curve of the sample is shown Fig. 7. The dehydrogenated $LiBH_4/Li_3AlH_6$ composite can absorb 4.9 wt% of hydrogen after 300 min of rehydrogenation.

To understand the mechanism of rehydrogenation, XRD and FTIR analyses were carried out, and the results are shown in Fig. 8. XRD analysis results show that the characteristic diffraction peaks of LiAl and AlB_2 disappear while the characteristic diffraction peaks of $LiBH_4$ and Al appear in the rehydrogenated samples. The FTIR analysis results (Fig. 8b) show that the B–H bond that disappeared after dehydrogenation reappear in the rehydrogenation sample, indicating the reformation of $LiBH_4$ during the rehydrogenation process. Based on the above analysis, we conclude that the dehydrogenated products contain LiAl, LiH, and AlB_2 (Fig. 5) and turn into $LiBH_4$ and Al (Fig. 8) under 8 MPa H_2 at 400 °C. The rehydrogenation process is as follows:

$$1/2AlB_2 + 1/2LiAl + 7/2LiH + 7/4H_2 \rightarrow LiBH_4 + 3LiH + Al \quad (7)$$

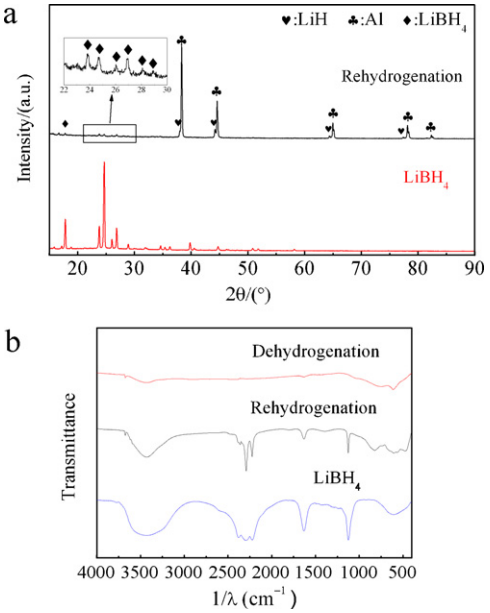

Fig. 8. (a) XRD patterns of rehydrogenated composite and (b) FTIR spectra of dehydrogenated and dehydrogenated composite.

The theoretical hydrogen absorption capacity for reaction 7 is 5.1 wt%, which is in good agreement with experimental results (4.9 wt%).

4. Conclusions

In summary, $LiBH_4/Li_3AlH_6$ composites without any additives exhibit superior hydrogen storage properties compared with $LiBH_4$ and Li_3AlH_6. The composite can release 8.5 wt% hydrogen below 500 °C. The dehydrogenation pathway for the $LiBH_4/Li_3AlH_6$ composite was identified by XRD, FTIR, and TG/DSC/MS analyses as:

(1) $Li_3AlH_6 \rightarrow 3LiH + Al + 3/2H_2$;
(2) $LiBH_4 + 1/2Al \rightarrow 1/2[Li_2B_2AlH_4] \rightarrow x/2(AlB_2 + 2LiH + 3H_2) + (1-x)/2[Li_2B_2AlH_4]$, $0 < x < 1$;
(3) $1/2LiH + 1/2Al \rightarrow 1/2LiAl + 1/4H_2$, $(1-x)/2[Li_2B_2AlH_4] \rightarrow (1-x)/2\ (AlB_2 + 2LiH + 3H_2)$, $0 < x < 1$.

The dehydrogenated composite can be rehydrogenated under 8 MPa at 400 °C, and the reversible hydrogen storage capacity of the composite reaches 4.9 wt%. The reversible hydrogenation/dehydrogenation process is found to be as follows:

$$LiBH_4 + 3LiH + Al \leftrightarrow 1/2AlB_2 + 1/2LiAl + 7/2LiH + 7/4H_2 \quad (8)$$

Acknowledgments

This work was supported by the National Basic Research Program of China (973 Program) (NO. 2010CB631304), National Natural Science Foundation of China (NO. 51171168 and 50671094) and Zhejiang Provincial Natural Science Foundation of China (NO. Y4110147).

References

[1] http://www1.eere.energy.gov/hydrogenandfuelcells/storage/pdfs/targets_onboard_hydro_storage_explanation.pdf, 2009.
[2] L. Schlapbach, A. Zuttel, Nature 414 (2001) 353–358.
[3] P. Chen, Z.T. Xiong, J.Z. Luo, J.Y. Lin, K.L. Tan, Nature 420 (2002) 302–304.
[4] C. Liang, Y.F. Liu, Y. Jiang, Z.J. Wei, M.X. Gao, H.G. Pan, Q.D. Wang, Phys. Chem. Chem. Phys. 13 (2011) 314–321.
[5] F. Fang, Y.T. Li, Y. Song, D.L. Sun, Q.G. Zhang, L.Z. Ouyang, M. Zhu, J. Phys. Chem. C 115 (2011) 13528–13533.
[6] C. Liang, Y.F. Liu, H.L. Fu, Y.F. Ding, M.X. Gao, H.G. Pan, J. Alloys Compd. 509 (2011) 7844–7853.
[7] P. Ngene, R. Van Den Berg, M.H.W. Verkuijlen, K.P. De Jong, P.E. De Jongh, Energy Environ. Sci. 4 (2011) 4108–4115.
[8] A. Ampoumogli, T. Steriotis, P. Trikalitis, D. Giasafaki, E.G. Bardaji, M. Fichtner, G. Charalambopoulou, J. Alloys Compd. 509 (2011) S705–S708.
[9] X.L. Zheng, G.T. Wu, W. Li, Z.T. Xiong, T. He, J.P. Guo, H. Chen, P. Chen, Energy Environ. Sci. 4 (2011) 3593–3600.
[10] J.A. Teprovich, D.A. Knight, M.S. Wellons, R. Zidan, J. Alloys Compd. 509 (2011) S562–S566.
[11] B.J. Zhang, B.H. Liu, Z.P. Li, J. Alloys Compd. 509 (2011) 751–757.
[12] W.F. Luo, D. Cowgill, K. Steward, V. Stavila, J. Alloys Compd. 497 (2010) L17–L20.
[13] F.C. Gennari, J.A. Puszkiel, J. Power Sources 195 (2010) 3266–3274.
[14] F.C. Gennari, L.F. Albanesi, J.A. Puszkiel, P.A. Larochette, Int. J. Hydrogen Energy 36 (2011) 563–570.
[15] M. Au, R.T. Walters, Int. J. Hydrogen Energy 35 (2010) 10311–10316.
[16] R.G. Chen, X.H. Wang, L. Xu, H. Li, C.P. Chen, L.X. Chen, H.G. Pan, J. Alloys Compd. 509 (2011) 3481–3485.
[17] A. Zuttel, P. Wenger, S. Rentsch, P. Sudan, P. Mauron, C. Emmenegger, J. Power Sources 118 (2003) 1–7.
[18] K. Miwa, N. Ohba, S. Towata, Y. Nakamori, S. Orimo, Phys. Rev. B 69 (2004) 245120.
[19] R.G. Chen, X.H. Wang, L.X. Chen, S.Q. Li, H.W. Ge, Y.Q. Lei, C.P. Chen, J. Alloys Compd. 495 (2010) 17–22.
[20] F. Buchter, Z. Lodziana, P. Mauron, A. Remhof, O. Friedrichs, A. Borgschulte, A. Zuttel, D. Sheptyakov, T. Strassle, A.J. Ramirez-Cuesta, Phys. Rev. B 78 (2008) 094302.
[21] B.C. Weng, X.B. Yu, Z. Wu, Z.L. Li, T.S. Huang, N.X. Xu, J. Ni, J. Alloys Compd. 503 (2010) 345–349.
[22] P. Mauron, F. Buchter, O. Friedrichs, A. Remhof, M. Bielmann, C.N. Zwicky, A. Zuttel, J. Phys. Chem. B 112 (2008) 906–910.
[23] J. Yang, A. Sudik, C. Wolverton, J. Phys. Chem. C 111 (2007) 19134–19140.
[24] O. Friedrichs, J.W. Kim, A. Remhof, F. Buchter, A. Borgschulte, D. Wallacher, Y.W. Cho, M. Fichtner, K.H. Oh, A. Zuttel, Phys. Chem. Chem. Phys. 11 (2009) 1515–1520.
[25] X.D. Kang, P. Wang, L.P. Ma, H.M. Cheng, Appl. Phys. A 89 (2007) 963–966.
[26] S.A. Jin, J.H. Shim, Y.W. Cho, K.W. Yi, O. Zabara, M. Fichtner, Scr. Mater. 58 (2008) 963–965.
[27] J.F. Mao, Z.P. Guo, H.K. Liu, X.B. Yu, J. Alloys Compd. 487 (2009) 434–438.
[28] J.K. Yang, X.H. Wang, J. Mao, L.X. Chen, H.G. Pan, S.Q. Li, H.W. Ge, C.P. Chen, J. Alloys Compd. 494 (2010) 58–61.
[29] J.W. Jang, J.H. Shim, Y.W. Cho, B.J. Lee, J. Alloys Compd. 420 (2006) 286–290.
[30] J.H. Shim, G.J. Lee, B.J. Lee, Y.J. Oh, Y.W. Cho, Catal. Today 120 (2007) 292–297.
[31] X.H. Wang, C.P. Chen, C.S. Wang, Q.D. Wang, J. Alloys Compd. 232 (1996) 192–196.
[32] X.H. Wang, R.G. Chen, Y. Zhang, C.P. Chen, Q.D. Wang, J. Alloys Compd. 420 (2006) 322–325.
[33] X.H. Wang, Y.Y. Bei, X.S. Song, G.H. Fang, S.Q. Li, C.P. Chen, Q.D. Wang, Int. J. Hydrogen Energy 32 (2007) 4011–4015.
[34] J.P. Soulie, G. Renaudin, R. Cerny, K. Yvon, J. Alloys Compd. 346 (2002) 200–205.
[35] D. Blanchard, H.W. Brinks, B.C. Hauback, P. Norby, Mater. Sci. Eng. B 108 (2004) 54–59.
[36] Y. Zhang, Q.F. Tian, J. Zhang, S.S. Liu, L.X. Sun, J. Phys. Chem. C 113 (2009) 18424–18430.
[37] M. Au, A. Jurgensen, J. Phys. Chem. B 110 (2006) 7062–7067.